Mapping Protein-Ligand Interactions in the Gas Phase Using a Functional Group Replacement Strategy. Comparison of CID and BIRD Activation Methods

Lu Deng, Elena N. Kitova, and John S. Klassen*

Department of Chemistry and Alberta Glycomics Centre, University of Alberta, Edmonton, Alberta, Canada T6G 2G2

Email: john.klassen@ualberta.ca

Abstract

Intermolecular interactions in the gaseous ions of two protein-ligand complexes, a single chain antibody (scFv) and its trisaccharide ligand (α-D-Gal*p*-(1→2)-[α-D-Abe*p*-(1→3)]-α-Man*p*-OCH_3, L1) and streptavidin homotetramer (S_4) and biotin (B), were investigated using a collision-induced dissociation (CID)-functional group replacement (FGR) strategy. CID was performed on protonated ions of a series of structurally related complexes based on the (scFv + L1) and (S_4 + 4B) complexes, at the +10 and +13 charge states, respectively. Intermolecular interactions were identified from decreases in the collision energy required to dissociate 50% of the reactant ion (E_{c50}) upon modification of protein residues or ligand functional groups. For the $(scFv + L1)^{10+}$ ion, it was found that deoxygenation of L1 (at Gal C3 and C6 and Man C4 and C6) or mutation of His101 (to Ala) resulted in a decrease in E_{c50} values. These results suggest that the four hydroxyl groups and His101 participate in intermolecular H-bonds. These findings agree with those obtained using the blackbody infrared radiative dissociation (BIRD)-FGR method. However, the CID-FGR method failed to reveal the relative strengths of the intermolecular interactions or establish Man C4 OH and His101 as a H-bond donor/acceptor pair. The CID-FGR method correctly identified Tyr43, but not Ser27, Trp79 and Trp120, as a stabilizing contact in the $(S_4 + 4B)^{13+}$ ion. In fact, mutation of Trp79 and Trp120 led to an increase in the Ec50 value. Taken together, these results suggest that the CID-FGR method, as implemented here, does not represent a reliable approach for identifying interactions in the gaseous protein-ligand complexes.

Introduction

Most biological processes, including the immune response, cell-cell communication, inflammation, and bacterial and viral infection, are dependent on the formation of non-covalent protein interactions. [1] The structure and stability of these complexes are determined by the concerted action of many forces (e.g. hydrogen (H-) bonds, ionic and van der Waals interactions) between binding partners and from the displacement and reorganization of solvent molecules associated with the binding partners. [2] An understanding of these forces and the structures they lead to is essential to a complete description of biochemical processes. Gas-phase studies of desolvated protein-ligand complexes afford an opportunity to probe their intrinsic properties, free of solvent effects. In principle, insights into the role of solvent in biomolecular recognition may be gained from a comparison of the stabilities of protein-ligand complexes in their hydrated and dehydrated states. However, for this approach to be successful, the dominant stabilizing intermolecular interaction in solution must be preserved upon desolvation. Blackbody infrared radiative dissociation (BIRD) [3-4], a thermal dissociation technique implemented with a Fourier-transform ion cyclotron resonance (FTICR) mass spectrometer, combined with a functional group replacement (FGR) strategy is arguably the most reliable method for identifying individual interactions in gaseous biological complexes and quantifying the strength of these interactions. [2,5-10] To establish whether a particular residue (on protein) or functional group (on ligand) is involved in binding, the group is modified (chemically or biochemically) in such a way that any pre-existing interaction is lost. The Arrhenius activation energy (E_a) for the loss of ligand from the modified complex is then compared to the E_a for ligand loss from the unmodified complex. A decrease in E_a indicates that the particular residue/functional group (that was modified) was involved in stabilizing the complex. Moreover, the difference in E_a for the

modified and unmodified complexes, *i.e.* $\Delta E_a = E_a(\text{unmodified}) - E_a(\text{modified})$, provides a measure of the strength of the interaction. Ideally, to identify interaction pairs (e.g. H-bond donor/acceptor pairs), a three step approach is utilized, in which E_a values are determined for complexes with modified ligand, modified protein and modified protein and ligand. For a given interaction pair, the E_a values determined for the three complexes are expected to be identical.

Using the BIRD-FGR method, the intermolecular interactions in the gaseous ions of three protein-ligand complexes: a single chain antibody (scFv), a model carbohyhdrate binding protein, and a trisaccharide ligand (α-D-Gal*p*-(1→2)-[α-D-Abe*p*-(1→3)]-α-Man*p*-OCH_3, L1) [2,5-6], β-lactoglobulin (Lg), a water-soluble whey protein possessing a large hydrophobic cavity, and fatty acids (FAs) [7-9] and the high affinity interaction involving the streptavidin homotetramer (S_4) and biotin (B) [10], were recently elucidated. Results obtained for protonated $(\text{scFv} + \text{L1})^{n+}$ ions revealed that some of the specific intermolecular H-bonds are conserved upon transfer of the complex from solution to the gas phase by electrospray ionization (ESI) [2]. Kinetic data measured for the loss of FA from deprotonated $(\text{Lg} + \text{FA})^{7-}$ ions suggest that the acyl chains of the FAs are retained within the hydrophobic cavity of Lg in the gas phase [7]. Furthermore, a comparison of the dissociation rate constants measured at 25°C in the gas phase and in aqueous solution revealed that (Lg + FA) complexes are more stable kinetically in the absence of water [8]. Kinetic data for ligand loss from the protonated $(S_4 + 4B)^{n+}$ ions, together with the results of molecular dynamics (MD) simulations, suggested that the solution specific intermolecular H-bonds and van der Waals contacts are preserved in the gas phase. [10] Moreover, the differences in dissociative E_a values measured for the gaseous complex ions and hydrated (S_4 + 4B) complex can be accounted for by the rehydration of B in the dissociative transition state (*TS*). [10]

The aforementioned studies highlight the power of the BIRD-FGR method to reveal new insights, inaccessible by other methods, into the forces responsible for the structure and kinetic stability of protein-ligand complexes. However, application of the BIRD-FGR method requires access to a FTICR mass spectrometer equipped with a temperature-controlled ion cell. Additionally, the determination of Arrhenius activation parameters requires kinetic measurements performed over a range of temperatures, which can be time consuming, especially at low reaction temperatures where the kinetics are slow. Consequently, there is interest in adapting the BIRD-FGR method for use with other, more readily available activation techniques, such as collision-induced dissociation (CID) [11]. For example, Douglas and coworkers described a CID-based approach to measure the energies required to dissociate the gas-phase ions of complexes of small-molecule inhibitors bound to the wild type (WT) form and single point binding site mutants (Asn44Ala, Gln87Met, and Gln87Tyr) of the catalytic domain of Cex, an enzyme that hydrolyses xylan and xylo-oligosaccharides. The authors found that the dissociation energies followed the same trend as the thermodynamic stabilities in aqueous solution and it was concluded that specific intermolecular H-bonds (involving residues Asn44 and Gln87) were preserved in the gas phase. [12] More recently, Oldham and coworkers described the results of a CID study on the complexes of a series of mutants of the FK506-binding protein (FKBP) and its ligand FK506. [13] Collisional activation of (FKBP + FK506) ions composed of WT or mutant proteins (Asp37Gly and Tyr82Phe) revealed that the removal of native protein–ligand interactions formed between residues Asp37 and Tyr82, and FK506 significantly destabilized the gas-phase complex. That the gas-phase results agreed qualitatively with the trend in affinities was presented as evidence for the preservation of specific interactions in the desolvated WT complex.

The results of these CID-FGR studies are very promising. However, the reliability of this general approach for identifying intermolecular interactions in gaseous protein-ligand complexes remains unclear. With this in mind, energy-resolved CID measurements were performed on protonated ions of a series of structurally related complexes based on (scFv + L1) and (S_4 + 4B). Intermolecular interactions were identified from decreases in the collision energy required to dissociate 50% of the reactant ion (i.e., Ec_{50}) upon modification of residues or functional groups that could participate in intermolecular interactions. The interactions were then compared to interaction maps generated using the BIRD-FGR approach (Figure 1) in order to test the reliability of the CID-FGR method.

Experimental Section

Proteins and ligands

Equine heart cytochrome *c* (cyto *c*, MW 12 358 Da), bovine β-lactoglobulin (Lg, MW 18 363 Da) and hen egg white avidin (Avidin, MW 15 636 Da) were purchased from Sigma-Aldrich Canada (Oakville, Canada). Stock solutions of cyto *c*, Lg, and Avidin (100 µM) were prepared by exchanging each protein into 100 mM ammonium acetate using Vivaspin 500 centrifugal concentrators with a 10 kDa MW cut-off (Sartorius Steddin Biotech, Gottingen, Germany). The recombinant scFv (MW 26 539 Da) of the monoclonal antibody Se155-4 and the single-point binding site mutant, His101Ala, were expressed in *E. coli* and isolated and purified using procedures described previously. [14-15] The plasmid for natural core streptavidin (containing residues 13-139 of WT streptavidin, monomer MW 13 271 Da) was a gift from Prof. P. Stayton (University of Washington). The single-point binding site mutants, Ser27Ala, Tyr43Ala Trp79Phe, Trp108Phe and Trp120Phe, were prepared using site-directed mutagenesis. The WT and mutant streptavidin proteins were expressed in *E. coli* and purified using procedures

described elsewhere.[16] Solutions of purified protein were exchanged directly into 100 mM aqueous ammonium acetate using an Amicon microconcentrators with a 10 kDa MW cut-off (Millipore Corp., Billerica, MA) and lyophilized. Protein (scFv or S_4) stock solutions were prepared at a concentration of 100 μM in 50 mM aqueous ammonium acetate (pH 6.8) and stored at -20 °C until needed.

The synthetic trisaccharide ligands, α-D-Gal*p*-(1→2)-[α-D-Abe*p*-(1→3)]-α-Man*p*-OCH_3 (L1, MW 486.5 Da), 3-deoxy-α-D-Gal*p*-(1→2)-[α-D-Abe*p*-(1→3)]-α-D-Man*p*-OCH_3 (L2, MW 470.5 Da), 6-deoxy-α-D-Gal*p*-(1→2)-[α-D-Abe*p*-(1→3)]-α-D-Man*p*-OCH_3 (L3, MW 470.5 Da), α-D-Gal*p*-(1→2)-[α-D-Abe*p*-(1→3)]-4-deoxy-α-D-Man*p*-OCH_3 (L4, MW 470.5 Da), α-D-Gal*p*-(1→2)-[α-D-Abe*p*-(1→3)]-6-deoxy-α-D-Man*p*-OCH_3 (L5, MW 470.5 Da), were gifts from Prof. D. Bundle (University of Alberta). Biotin (B, MW 244.3 Da) was purchased from Sigma-Aldrich Canada (Oakville, Canada). Ligand stock solutions were prepared at a concentration of 200 μM in Milli-Q water and stored at -20 °C until needed.

To produce gaseous protonated $(scFv + L)^{n+}$ ions, ESI was performed on solutions containing WT scFv (8 μM) (or WT scFv and His101Ala scFv (10 μM)), and L (5 - 15 μM) in 10 mM ammonium acetate (pH 6.8). The concentrations of protein and ligand were adjusted to minimize the formation of nonspecific (scFv + L) complexes during the ESI process. [17] The gaseous WT $(S_4 + 4B)^{n+}$ and mutant $(S_4 + 4B)^{n+}$ ions were produced by ESI performed on solutions containing WT S_4 (8 μM) and one of the mutants S_4 (10 μM), and B (80 μM) in 10 mM ammonium acetate (pH 6.8). Imidazole (5 mM) was added to reduce charge state for the gaseous $(S_4 + 4B)^{n+}$ ions so as to enhance the abundance of the $(S_4 + 4B)^{13+}$ ion. [18] For the ion mobility

separation (IMS) measurements, ESI was performed on solutions (10 μM) of each calibrant protein (cyto *c*, Lg, and Avidin) in 10 mM ammonium acetate (pH 6.8).

Mass spectrometry

Measurements were performed using a Synapt G2-S quadrupole-ion mobility separation-time of flight (Q-IMS-TOF) mass spectrometer (Waters, UK), equipped with a nanoflow ESI (nanoESI) ion source. NanoESI was performed using borosilicate tubes (1.0 mm o.d., 0.68 mm i.d.), pulled to ~5 μm o.d. at one end using a P-97 micropipette puller (Sutter Instruments, Novato, CA). The electric field required to spray the solution in positive ion mode was established by applying a voltage of 1.0 – 1.6 kV to a platinum wire inserted inside the nanoESI tip. The solution flow rate was typically ~20 nL min^{-1}. A cone voltage of 30 V was used and the source block temperature was maintained at 80 ºC. The gaseous protein-ligand complexes, at the desired charge states, were isolated using the quadrupole mass filter. CID of the isolated ions was carried out in the Trap region using Ar as the collision gas. A series of CID experiments were performed on the $(scFv + L)^{+10}$ ions at different trap pressures (P_{trap} = 4, 6 and 8) to investigate the influence of collision gas pressure on the CID results. For all other measurements, an Ar pressure of 2.1 x 10^{-2} mbar (P_{trap} = 6) was used. The collision energy was controlled by adjusting the Trap collision energy voltage. Data were acquired at 5 V increments; at collision regions corresponding to ~50% dissociation, data were collected at 1 V increments to ensure more precise determination of Ec_{50} values. The TOF-MS was operated over a *m/z* range of 50 to 8000 at a pressure of 1.2 x 10^{-6} mbar. Three replicate measurements (using 1 min acquisition times) were performed at each collision energy.

To identify small differences in the Ec_{50} values for complexes composed of WT and mutant protein, the CID measurements were performed simultaneous on complexes of WT and a given mutant (e.g. WT $(scFv + L1)^{10+}$ and His101Ala $(scFv+ L1)^{10+}$; WT $(S_4 + 4B)^{13+}$ and Try43Ala $(S_4 + 4B)^{13+}$). For these measurements, ESI was performed on solutions containing both mutant and WT protein at concentrations that yielded similar intensities for the ions of interest. Quadrupole isolation of each complex was carried out in an alternating fashion. This approach was adopted in order to minimize uncertainty in the Ec_{50} values resulting from fluctuations in instrumental conditions.[19] A similar approach could not be implemented for the comparison of Ec_{50} values for (scFv + L) complexes composed of L1 and the monodeoxy analogs (L2 - L5) because of the small difference in the *m/z* values. For this reason, the CID measurements were carried out on each complex individually.

IMS measurements on the WT $(scFv + L1)^{n+}$ ions were performed with a fixed wave height of 35 V and velocity of 1200 m s^{-1}. The Trap and Transfer collision energies were maintained at 5 V and 2 V, respectively. The bias on Trap DC was 40 V. Ar was used in the Trap and Transfer ion guides at a pressure of 2.97 x 10^{-2} mbar and 3.04 x 10^{-2} mbar, respectively. The helium chamber preceding the traveling wave ion mobility (TWIMS) device was operated with a He flow rate of 140 mL min^{-1}. All traveling-wave IMS measurements were performed using N_2 as the mobility gas at a flow rate of 40 mL min^{-1} and pressure of 8.90 mbar. Determination of the collision cross section (Ω) from drift time measurements was carried out using protocols described elsewhere. [10,20-21] Briefly, proteins (cyto *c*, Lg, and Avidin) with known Ω (in He) were analysed under the same experimental conditions (as for the $(scFv + L1)^{n+}$ ions) to establish a correlation between the measured drift times (t_D) and Ω. A linear calibration curve of literature Ω values versus corrected t_D was generated with an R^2 value of 0.994, Figure S1 (Supplementary

Material). The Ω values of the protonated (scFv + L1)$^{n+}$ ions were then determined from the calibration curve and the corresponding t_D values. The Ω for the reported (scFv + L1) crystal structure (protein ID: 1MFA) [14] was calculated using Mobcal [22] and the trajectory method.

CID date analysis

Dissociation profiles were constructed from the percentage precursor remaining (%precursor) as a function of collision energy. At each collision energy, %precursor was calculated using eq 1:

$$\%\text{precursor} = \frac{Ab_{\text{precursor}}}{Ab_{\text{precursor}} + \sum Ab_{\text{product}}} \times 100 \quad (1)$$

where $Ab_{\text{precursor}}$ and $\sum Ab_{\text{product}}$ are the abundances of the precursor ion and the sum of the abundances of all product ions, respectively. The dissociation profiles were treated as sigmoid curves using Origin 8 (OriginLab, Northampton, MA) by eq 2:

$$\%\text{precursor} = \frac{a}{1 + \mathrm{e}^{-k(\mathrm{Ec} - x_c)}} \times 100 \quad (2)$$

where a is the amplitude, k is the coefficient and x_c is the center of the sigmoid function. From each dissociation profile, the corresponding parameters (a, k and x_c) and associated uncertainties (δa, δk and δx_c) were determined.

The collision energy required to dissociate 50% of the reactant ion (i.e., the Ec_{50} values) were then calculated by eq 3:

$$\mathrm{Ec}_{50} = -k^{-1} \ln(2a - 1) + x_c \quad (3)$$

The uncertainties of Ec_{50} values (δEc_{50}) were calculated from error propagation and eq 4:

$$\delta \mathrm{Ec}_{50} = \left|\frac{\mathrm{dEc}_{50}}{\mathrm{d}k}\right| \delta k + \left|\frac{\mathrm{dEc}_{50}}{\mathrm{d}a}\right| \delta a + \left|\frac{\mathrm{dEc}_{50}}{\mathrm{d}x_c}\right| \delta x_c \quad (4)$$

Results and discussion

Mapping the intermolecular interactions in the (scFv + L1)$^{10+}$ ion

Protonated gas-phase ions of the (scFv + L) complexes composed of WT scFv and native trisaccharide ligand (L1) or monodeoxy analogs (L2 – L5) were produced by ESI performed on aqueous ammonium acetate solutions (10 mM, pH 6.8) containing WT scFv (8 µM) and L (5 - 10 µM). Abundant protonated ions of ligand-bound and unbound scFv were detected, e.g. scFv $^{n+}$ and (scFv + L)$^{n+}$ ions at n = 9 – 11. Notably, there was no evidence of nonspecific ligand binding to scFv under the experimental conditions used. An illustrative ESI mass spectrum acquired for a solution of scFv and L1 is shown in Figure S2. Also shown are the corresponding arrival time distributions measured for the (scFv + L1)$^{n+}$ ions. The narrow charge state distribution is suggestive of a compact protein structure in the gas phase. This conclusion is further supported by the results of the IMS measurements performed on the (scFv + L1)$^{n+}$ ions. The Ω values for the (scFv + L1)$^{n+}$ ions, at charge states 9 - 11, which were determined from their measured t_D and the calibration curve, are listed in Table S1, together with the Ω value estimated for the crystal structure of (scFv + L1) (protein ID: 1MFA)[14] using Mobcal [22] and the trajectory method. The Ω values measured for the (scFv + L1)$^{n+}$ ions exhibit only a very subtle dependence on charge state, suggesting that charge-induced structural changes are minimal, at least at these charge states. The average Ω value for the (scFv + L1)$^{n+}$ ions (22.3 ± 0.4 nm^2) agrees within 4% with the Ω value estimated for the (scFv + L1) crystal structure (23.2 ± 0.4 nm^2). From this it is concluded that the transfer of the (scFv + L1) complex (and presumably the other (scFv + L)

complexes) from neutral aqueous solution to the gas phase by ESI (in positive ion mode) is not accompanied by significant structural changes.

The +10 charge state of the (scFv + L) complexes was selected for all of the CID measurements. A representative CID mass spectrum for the $(scFv + L1)^{10+}$ ion is shown in Figure 2a; for comparison purposes a BIRD mass spectrum is shown in Figure 2b. CID of the protonated $(scFv + L)^{10+}$ ions in the Trap region led exclusively to the formation of the $scFv^{10+}$ ion (produced by the loss of neutral L); the $scFv^{9+}$ ion (produced by the loss of charge ligand) was detected but with low abundance. The absence $(L1 + H)^+$ ion in any of the CID spectra, taken together with the appearance of $(L1 + Na)^+$ and $(L1 + K)^+$ ions, suggests that the $scFv^{9+}$ ion is produced from metal ion adducts of $(scFv + L1)^{10+}$ that were not completely removed by quadrupole isolation. These results are consistent with the findings of the BIRD study. [2]

Shown in Figure 3a are CID dissociation profiles (as a function of collision energy) measured for the $(scFv + L)^{10+}$ ions composed WT scFv and L1 – L5. The Ec_{50} values determined for each of the $(scFv + L)^{10+}$ ions are listed (Table 1). For comparison purposes, the corresponding Arrhenius parameters are also included. The stabilizing role of individual ligand hydroxyl groups was established from the difference in Ec_{50} values (ΔEc_{50}) determined for $(scFv + L1)^{10+}$ and the corresponding $(scFv + L)^{10+}$ ions containing one of the monodeoxy analogs (L2 – L5) (Table 1). In all four cases, deoxygenation of L1 led to a significant decrease in Ec_{50}. The corresponding ΔEc_{50} values are: 26.2 ± 1.8 eV (L2), 15.8 ± 1.9 eV (L3), 29.3 ± 2.1 eV (L4) and 33.1 ± 1.8 eV (L5). These results suggest that all four hydroxyl groups participate in intermolecular H-bonds that stabilize the $(scFv + L1)^{10+}$ ion. Importantly, these results are qualitatively consistent with those of the BIRD study, in which deoxygenation at each of the four sites resulted in a measurable decrease in the dissociation E_a. [2] However, the trend in ΔEc_{50}

values (L5 > L4 > L2 > L3) does not match the trend in ΔE_a values (L5 ≈ L2 > L3 ≈ L4). This finding is discussed in more detail below.

The aforementioned results were acquired using an Ar pressure of 2.1 x 10^{-2} mbar (P_{trap} = 6). It was of interest to assess whether the collision gas pressure has any influence on the trend in Ec_{50} values. To answer this question, measurements were repeated at Ar pressures of 1.5 x 10^{-2} mbar (P_{trap} = 4) and 2.7 x 10^{-2} mbar (P_{trap} = 8). Shown in Figure S3a and S3b are the CID dissociation profiles measured at P_{trap} 4 and 8, respectively. The Ec_{50} values and corresponding ΔEc_{50} values are listed in Table S2. Inspection of the results reveals that the collision gas pressure does have a modest influence the relative magnitude of the ΔEc_{50} values (P_{trap} = 4: L5 ≈ L4 > L2 > L3; P_{trap} = 8: L5 ≈ L4 > L2 ≈ L3). Notably, however, the trends in ΔEc_{50} values established at P_{trap} 4 and 8 do not match the trend in ΔE_a values.

To perform the CID measurements on the $(scFv + L)^{10+}$ ions composed of the His101Ala mutant, protonated gas-phase ions $(scFv + L)^{n+}$ of both WT and His101Ala were produced simultaneously by ESI performed on aqueous ammonium acetate solutions (10 mM, pH 6.8) of WT scFv (8 µM), His101Ala scFv (10 µM), and L1 or L4 (10-15 µM). Pairs of CID profiles are shown in Figure 3b and the corresponding Ec_{50} values are listed (Table 1); the Arrhenius parameters are also included in Table 1. Comparison of the dissociation profiles for the $(scFv + L1)^{10+}$ ions composed of WT and His101Ala reveals that mutation of His101 results in a reduction, albeit small (5.9 eV), in Ec_{50} suggesting that the side chain of the residue is involved in stabilizing the complex (presumably through an intermolecular H-bond). It was previously shown using the BIRD-FGR method that the side chain of His101 is engaged in a H-bond with the OH group at the C4 position of Man. [2] Notably, this interaction is also identified in the crystal structure of the (scFv + L1) complex. [14] Interestingly, deoxygenation at the Man C4

position results in a further (and significant) decrease in Ec_{50} (by 24.4 eV). Taken together, these results suggest that both His101 and Man C4 OH stabilize the complex, but not through a common interaction(s). In contrast, similar ΔE_a values were obtained from BIRD measurements performed on the $(scFv + L1)^{10+}$ ions upon deoxygenation (at Man C4) or mutation of His101 (to Ala) and upon simultaneous deoxygenation and mutation. [2]

The CID results obtained for the $(scFv + L)^{10+}$ ions results reveal that the loss of intermolecular H-bonds in the $(scFv + L)^{10+}$ ion results in measurable decreases in the Ec_{50} values. However, the magnitude of the changes in Ec_{50} values (i.e., ΔEc_{50}) does not reflect the relative E_a values. The lack of agreement between the relative Ec_{50} and E_a values can be explained by the fact that a CID mass spectrum reflects the microcannonical dissociation rate constants convoluted over the internal energy distribution (which is expected to be non-Boltzmann in nature) of the reactant ion at a given collision energy. [23-24] At low internal energies the relative ordering of rate constants (for structurally related complexes) will tend to reflect the trend in dissociation E_a, while at high internal energies, the ordering of rate constants will be dominated by the trend in the pre-exponential (A) factors. In other words, the ΔEc_{50} values reflect differences in the dissociation kinetics over a range of internal energy distributions. It is, therefore, not surprising that there is no temperature at which the thermal dissociation rate constants (Figure S4) would lead to the observed trend of Ec_{50} values for the $(scFv + L)^{10+}$ ions, where L = L1 – L5. Moreover, the observation that the magnitude of the ΔEc_{50} values measured upon disruption of the His101/Man C4-OH H-bond is sensitive to the nature of the modification (i.e., mutation versus deoxygenation) is evidence that modifications that are energetically equivalent (i.e., give rise to the same change in E_a), are not necessarily equivalent in terms of Ec_{50} values. The larger decrease in Ec_{50} upon deoxygenation of L1 at Man C4, compared to

mutation of His101, is consistent with the reported differences in the kinetic stabilities of the WT $(scFv + L4)^{10+}$ and His101Ala $(scFv+L4)^{10+}$ ions (Figure S5). These kinetic differences are entropic in origin (since the E_a values are indistinguishable) and are believed to reflect the participation of the Man C4 OH group in intramolecular H-bond in the dissociative *TS*, which serves to rigidify the ligand (and decrease the entropy of activation) relative to the (scFv + L4) complex. [2]

Mapping the intermolecular interactions in the $(S_4 + 4B)^{13+}$ ion

To further test the reliability of the CID-FGR strategy, the method was used to probe the intermolecular interactions in protonated $(S_4 + 4B)^{13+}$ ions. Protonated $(S_4 + 4B)^{n+}$ ions, at n = 12 to 17, were produced by ESI from aqueous ammonium acetate solutions (10 mM, pH 6.8) containing WT S_4 (8 µM) and one of the binding site single point mutants (Trp79Phe, Trp108Phe, Trp120Phe, Ser27Ala or Tyr43Ala) (10 µM), B (80 µM) and imidazole (5 mM). An illustrative ESI mass spectrum is shown in Figure S6 for a solution containing both WT and Tyr43Ala and B. As reported elsewhere [10], the Ω values for the protonated WT $(S_4 + 4B)^{n+}$ ions, where n = 12 to 16, are independent of charge state, with an average value 35.0 ± 0.1 nm^2. This value agrees within 10% with the Ω value (38.4 ± 0.4 nm^2) estimated for the crystal structure of the $(S_4 + 4B)$ complex. Based on these results it was suggested that the transfer of $(S_4 + 4B)$ from neutral aqueous solution to the gas phase by ESI is not accompanied by large structural changes.[10]

CID of the $(S_4 + 4B)^{13+}$ ions composed of WT or mutant S_4 resulted predominantly in the loss of neutral B; the loss of protonated B was observed as a minor pathway (Figure 4). Subsequent dissociation of the primary product ions, $(S_4 + 3B)^{13+}$ and $(S_4 + 3B)^{12+}$, proceeded in a similar fashion, such that a series of $(S_4 + iB)^{13+}$ and $(S_4 + iB)^{12+}$ ions are evident in the CID

mass spectra (Figure 4). The CID dissociation profiles (for pairs of $(S_4 + 4B)^{13+}$ ions composed of WT and each single point mutant) are shown in Figure 5. The Ec_{50} values are reported in Table 2, along with the corresponding ΔEc_{50} values and the Arrhenius parameters [10]. Inspection of the values in Table 2 reveals that mutation of Tyr43 (to Ala) results in a small (4.0 eV) decrease in Ec_{50}, suggesting that this residue stabilizes the gaseous $(S_4 + 4B)^{13+}$ ion. This finding is consistent with the result of the BIRD-FGR mapping study. [10] In contrast, mutation of Ser27 (to Ala) produced no significant change in Ec_{50}. The apparent absence of an interaction at Ser27 is inconsistent with the BIRD-FGR results, which revealed a strong (~5 kcal mol^{-1}) interaction in the $(S_4 + 4B)^{13+}$ ion.[10] Unexpectedly, mutation of Trp79, Trp108 and Trp120 (to Phe) resulted in a small increase (3 – 4 eV) in Ec_{50}, suggesting that the mutations enhance the energetic stability of the gaseous complex. However, according to the BIRD results, replacement of Trp79 or Trp120 with Phe leads to a decrease in E_a (~2.5 kcal mol^{-1}) [10], while mutation of Trp108 (to Phe) does not change the E_a value. Taken together, these results reveal that the CID-FGR approach, when implemented using binding site mutants, lacks reliability and is prone to both false positives and false negatives.

Conclusions

The present study represents the first direct comparison of the CID-FGR and BIRD-FGR methods for mapping intermolecular interactions in the gaseous ions of protein-ligand complexes. The CID results obtained for protonated $(scFv + L1)^{10+}$ and $(S_4 + 4B)^{13+}$ ions demonstrate conclusively that structural modifications that lead to changes in the dissociation E_a do not necessarily lead to measurable changes in the Ec_{50} values. Similarly, changes in Ec_{50} are not always indicative of the loss of intermolecular interactions. Therefore, while the CID-FRG approach can, in some instances, correctly identify residues or functional groups that stabilize the

complex, the method is prone to both false positives and false negatives. It was also shown that the trend in Ec_{50} values for structurally related complexes do not necessarily correlate with the trends in E_a values or thermal rate constants. Moreover, protein mutation and ligand modification do not necessarily produce equivalent effects in terms of Ec_{50} values. The discrepancies between the CID-FGR and BIRD-FGR results can be explained qualitatively by the fact the CID dissociation curves reflect the dissociation rate constants, which are functions of both energy and entropy, convoluted over the internal energy distributions achieved over a range of collision energies. Taken together, the results of this study suggest that the CID-FGR method, as implemented here, does not represent a reliable approach for identifying intermolecular interactions in the gaseous ions of protein-ligand complexes.

Acknowledgement

The authors are grateful for financial support provided by the Natural Sciences and Engineering Research Council of Canada and the Alberta Glycomics Centre.

References

1. Kitova, E., El-Hawiet, A., Schnier, P., Klassen, J.: Reliable Determinations of Protein–Ligand Interactions by Direct ESI-MS Measurements. Are We There Yet? *J. Am. Soc. Mass Spectrom.* **23,** 431-441 (2012)

2. Kitova, E.N., Seo, M., Roy, P.-N., Klassen, J.S.: Elucidating the Intermolecular Interactions within a Desolvated Protein−Ligand Complex. An Experimental and Computational Study. *J. Am. Chem. Soc.* **130,** 1214-1226 (2008)

3. Price, W.D., Schnier, P.D., Jockusch, R.A., Strittmatter, E.F., Williams, E.R.: Unimolecular Reaction Kinetics in the High-Pressure Limit without Collisions. *J. Am. Chem. Soc.* **118,** 10640-10644 (1996)

4. Dunbar, R.C., McMahon, T.B.: Activation of Unimolecular Reactions by Ambient Blackbody Radiation. *Science* **279,** 194-197 (1998)

5. Kitova, E.N., Bundle, D.R., Klassen, J.S.: Thermal Dissociation of Protein−Oligosaccharide Complexes in the Gas Phase: Mapping the Intrinsic Intermolecular Interactions. *J. Am. Chem. Soc.* **124,** 5902-5913 (2002)

6. Kitova, E.N., Bundle, D.R., Klassen, J.S.: Partitioning of Solvent Effects and Intrinsic Interactions in Biological Recognition. *Angew. Chem. Int. Ed.* **43,** 4183-4186 (2004)

7. Liu, L., Bagal, D., Kitova, E.N., Schnier, P.D., Klassen, J.S.: Hydrophobic Protein−Ligand Interactions Preserved in the Gas Phase. *J. Am. Chem. Soc.* **131,** 15980-15981 (2009)

8. Liu, L., Michelsen, K., Kitova, E.N., Schnier, P.D., Klassen, J.S.: Evidence that Water Can Reduce the Kinetic Stability of Protein−Hydrophobic Ligand Interactions. *J. Am. Chem. Soc.* **132,** 17658-17660 (2010)

9. Liu, L., Michelsen, K., Kitova, E.N., Schnier, P.D., Klassen, J.S.: Energetics of Lipid Binding in a Hydrophobic Protein Cavity. *J. Am. Chem. Soc.* **134,** 3054-3060 (2012)

10. Deng, L., Broom, A., Kitova, E.N., Richards, M.R., Zheng, R.B., Shoemaker, G.K., Meiering, E.M., Klassen, J.S.: Kinetic Stability of the Streptavidin–Biotin Interaction Enhanced in the Gas Phase. *J. Am. Chem. Soc.* **134,** 16586-16596 (2012)

11. McLuckey, S.A.: Principles of collisional activation in analytical mass spectrometry. *J. Am. Soc. Mass Spectrom.* **3,** 599-614 (1992)

12. Tešić, M., Wicki, J., Poon, D.K.Y., Withers, S.G., Douglas, D.J.: Gas Phase Noncovalent Protein Complexes that Retain Solution Binding Properties: Binding of Xylobiose Inhibitors to the β-1, 4 Exoglucanase from Cellulomonas fimi. *J. Am. Soc. Mass Spectrom.* **18,** 64-73 (2007)

13. Hopper, J.T.S., Oldham, N.J.: Collision Induced Unfolding of Protein Ions in the Gas Phase Studied by Ion Mobility-Mass Spectrometry: The Effect of Ligand Binding on Conformational Stability. *J. Am. Soc. Mass Spectrom.* **20,** 1851-1858 (2009)

14. Zdanov, A., Li, Y., Bundle, D.R., Deng, S.J., MacKenzie, C.R., Narang, S.A., Young, N.M., Cygler, M.: Structure of a single-chain antibody variable domain (Fv) fragment complexed with a carbohydrate antigen at 1.7-A resolution. *Proc. Natl. Acad. Sci. U. S. A.* **91,** 6423-6427 (1994)

15. Bundle, D.R., Baumann, H., Brisson, J.-R., Gagne, S.M., Zdanov, A., Cygler, M.: The solution structure of a trisaccharide-antibody complex: comparison of NMR measurements with a crystal structure. *Biochemistry* **33,** 5183-5192 (1994)

16. Chilkoti, A., Tan, P.H., Stayton, P.S.: Site-directed mutagenesis studies of the high-affinity streptavidin-biotin complex: contributions of tryptophan residues 79, 108, and 120. *Proc. Natl. Acad. Sci. U.S.A.* **92,** 1754-1758 (1995)

17. Wang, W., Kitova, E.N., Klassen, J.S.: Nonspecific Protein−Carbohydrate Complexes Produced by Nanoelectrospray Ionization. Factors Influencing Their Formation and Stability. *Anal. Chem.* **77,** 3060-3071 (2005)

18. Sun, J., Kitova, E.N., Klassen, J.S.: Method for Stabilizing Protein−Ligand Complexes in Nanoelectrospray Ionization Mass Spectrometry. *Anal. Chem.* **79,** 416-425 (2006)

19. Hopper, J., Rawlings, A., Afonso, J., Channing, D., Layfield, R., Oldham, N.: Evidence for the Preservation of Native Inter- and Intra-Molecular Hydrogen Bonds in the Desolvated FK-Binding Protein·FK506 Complex Produced by Electrospray Ionization. *J. Am. Soc. Mass Spectrom.* **23,** 1757-1767 (2012)

20. Bush, M.F., Hall, Z., Giles, K., Hoyes, J., Robinson, C.V., Ruotolo, B.T.: Collision Cross Sections of Proteins and Their Complexes: A Calibration Framework and Database for Gas-Phase Structural Biology. *Anal. Chem.* **82,** 9557-9565 (2010)

21. Ruotolo, B.T., Benesch, J.L.P., Sandercock, A.M., Hyung, S.-J., Robinson, C.V.: Ion mobility-mass spectrometry analysis of large protein complexes. *Nat. Protocols* **3,** 1139-1152 (2008)

22. Mesleh, M.F., Hunter, J.M., Shvartsburg, A.A., Schatz, G.C., Jarrold, M.F.: Structural Information from Ion Mobility Measurements: Effects of the Long-Range Potential. *The Journal of Physical Chemistry* **100,** 16082-16086 (1996)

23. Vékey, K.: Internal Energy Effects in Mass Spectrometry. *J. Mass Spectrom.* **31,** 445-463 (1996)

24. Mayer, P.M., Poon, C.: The mechanisms of collisional activation of ions in mass spectrometry. *Mass Spectrom. Rev.* **28,** 608-639 (2009)

Table 1. Comparison of Ec_{50} with Arrhenius parameters (E_a, A) determined for the dissociation of $(scFv + L)^{10+}$ ions, where L = L1, L2, L3, L4 or L5, and WT scFv or the single point binding site mutant His101Ala.

scFv	Ligand	Ec_{50} [a] (eV)	ΔEc_{50} [b] (eV)	E_a [c] (kcal mol^{-1})	ΔE_a [d] (kcal mol^{-1})	A [c] (s^{-1})
WT	L1	238.2 ± 1.6	-	54.7 ± 0.6	-	$10^{27.9 \pm 0.7}$
WT	L2	212.0 ± 0.8	26.2 ± 1.8	46.5 ± 0.7	8.2 ± 0.9	$10^{24.2 \pm 0.4}$
WT	L3	222.4 ± 1.0	15.8 ± 1.9	48.5 ± 0.9	6.2 ± 1.1	$10^{25.0 \pm 0.5}$
WT	L4	208.9 ± 1.4	29.3 ± 2.1	49.9 ± 1.0	4.8 ± 1.2	$10^{25.8 \pm 0.6}$
WT	L5	205.1 ± 0.9	33.1 ± 1.8	46.1 ± 0.8	8.6 ± 1.0	$10^{24.0 \pm 0.4}$
His101Ala	L1	232.3 ± 1.8	5.9 ± 2.4	50.0 ± 0.3	4.7 ± 0.7	$10^{25.5 \pm 0.2}$
His101Ala	L4	207.9 ± 1.0	30.3 ± 1.8	49.4 ± 0.8	5.3 ± 1.0	$10^{25.4 \pm 0.4}$
			(24.4 ± 2.1) [e]		(0.6 ± 0.9) [f]	

a. Errors correspond to the uncertainties of Ec_{50} values (δEc_{50}) that were calculated using error propagation. b. $\Delta Ec_{50} = Ec_{50}(scFv+L1) - Ec_{50}(scFv+L)$; errors correspond to the uncertainties from error propagation. c. E_a and A values taken from refs [2],[6] and errors correspond to one standard deviation. d. $\Delta E_a = E_a(scFv+L1) - E_a(scFv+L)$; errors correspond to the uncertainties from error propagation. e. $\Delta Ec_{50} = Ec_{50}(His101Ala+L1) - Ec_{50}(His101Ala+L4)$; errors correspond to the uncertainties from error propagation. f. $\Delta E_a = E_a(His101Ala+L1) - E_a(His101Ala+L4)$; errors correspond to the uncertainties from error propagation.

Table 2. Comparison of Ec_{50} with Arrhenius parameters (E_a, A) determined for the loss of neutral B from the protonated $(S_4 + 4B)^{13+}$ ions, where S_4 = WT, Trp79Phe, Trp108Phe, Trp120Phe, Ser27Ala or Tyr43Ala.

S_4	Ec_{50} [a] (eV)	ΔEc_{50} [b] (eV)	E_a [c] (kcal mol^{-1})	ΔE_a [d] (kcal mol^{-1})	A [c] (s^{-1})
WT_1	394.2 ± 1.4	-	43.2 ± 1.1	-	$10^{23.2 \pm 0.6}$
Ser27Ala	392.7 ± 1.4	1.6 ± 1.9	38.5 ± 1.0	4.7 ± 1.4	$10^{20.7 \pm 0.6}$
WT_2	393.7 ± 1.3	-		-	
Tyr43Ala	389.6 ± 1.3	4.0 ± 1.9	37.8 ± 0.9	5.4 ± 1.4	$10^{20.4 \pm 0.5}$
WT_3	392.3 ± 2.3	-		-	
Trp79Phe	395.9 ± 1.1	-3.6 ± 2.5	40.7 ± 0.3	2.5 ± 1.1	$10^{21.8 \pm 0.2}$
WT_4	389.3 ± 1.7	-		-	
Trp108Phe	393.2 ± 1.5	-3.9 ± 2.3	44.8 ± 0.5	-1.6 ± 1.2	$10^{24.1 \pm 0.3}$
WT_5	397.2 ± 1.4	-		-	
Trp120Phe	400.9 ± 1.1	-3.7 ± 1.7	40.6 ± 0.4	2.6 ± 1.2	$10^{21.8 \pm 0.2}$

a. Errors correspond to the uncertainties of Ec_{50} values (δEc_{50}) that were calculated using error propagation. b. $\Delta Ec_{50} = Ec_{50}(WT) - Ec_{50}(mutant)$; errors correspond to the uncertainties from error propagation. c. E_a and A values taken from ref [10]; errors correspond to one standard deviation. d. $\Delta E_a = E_a(WT) - E_a(mutant)$; errors correspond to the uncertainties from error propagation.

Figure captions

Figure 1. Map of intermolecular interactions determined using BRID-FGR method for the protonated (a) $(scFv + L1)^{10+}$ and (b) $(S_4 + 4B)^{13+}$ ions. The maps were adapted from those reported in reference 2 and 10, respectively. In (b), the Trp120 residue is located on an adjacent subunit.

Figure 2. (a) CID mass spectrum acquired for the protonated $(scFv + L1)^{10+}$ ion with a collision energy of 240 eV. (b) BIRD mass spectrum obtained for the $(scFv + L1)^{10+}$ ion at reaction temperature of 154 °C and a reaction time of 6 s.

Figure 3. (a) CID profiles measured for the protonated WT $(scFv + L)^{10+}$ ions, where L= L1 – L5, at $P_{trap} = 6$ (b) CID profiles for the protonated His101Ala $(scFv + L1)^{10+}$ and His101Ala $(scFv + L4)^{10+}$ ions at $P_{trap} = 6$. Also shown are the CID profiles for the WT $(scFv + L1)^{10+}$ and $(scFv + L4)^{10+}$ ions. The solid curves were determined from sigmoid fitting to the collision energy-dependent %precursor values.

Figure 4. CID mass spectrum acquired for protonated $(S_4 + 4B)^{13+}$ ions, composed of (a) WT or (b) Tyr43Ala S_4, with a collision energy of 390 eV. The region from *m/z* 4300-4500 was magnified by a factor of 50.

Figure 5. CID profiles for pairs of protonated $(S_4 + 4B)^{13+}$ ions involving WT and (a) Ser27Ala, (b) Tyr43Ala, (c) Trp79Phe, (d) Trp108Phe, and (e) Trp120Phe. The solid curves were determined from sigmoid fitting to the collision energy-dependent %precursor values.

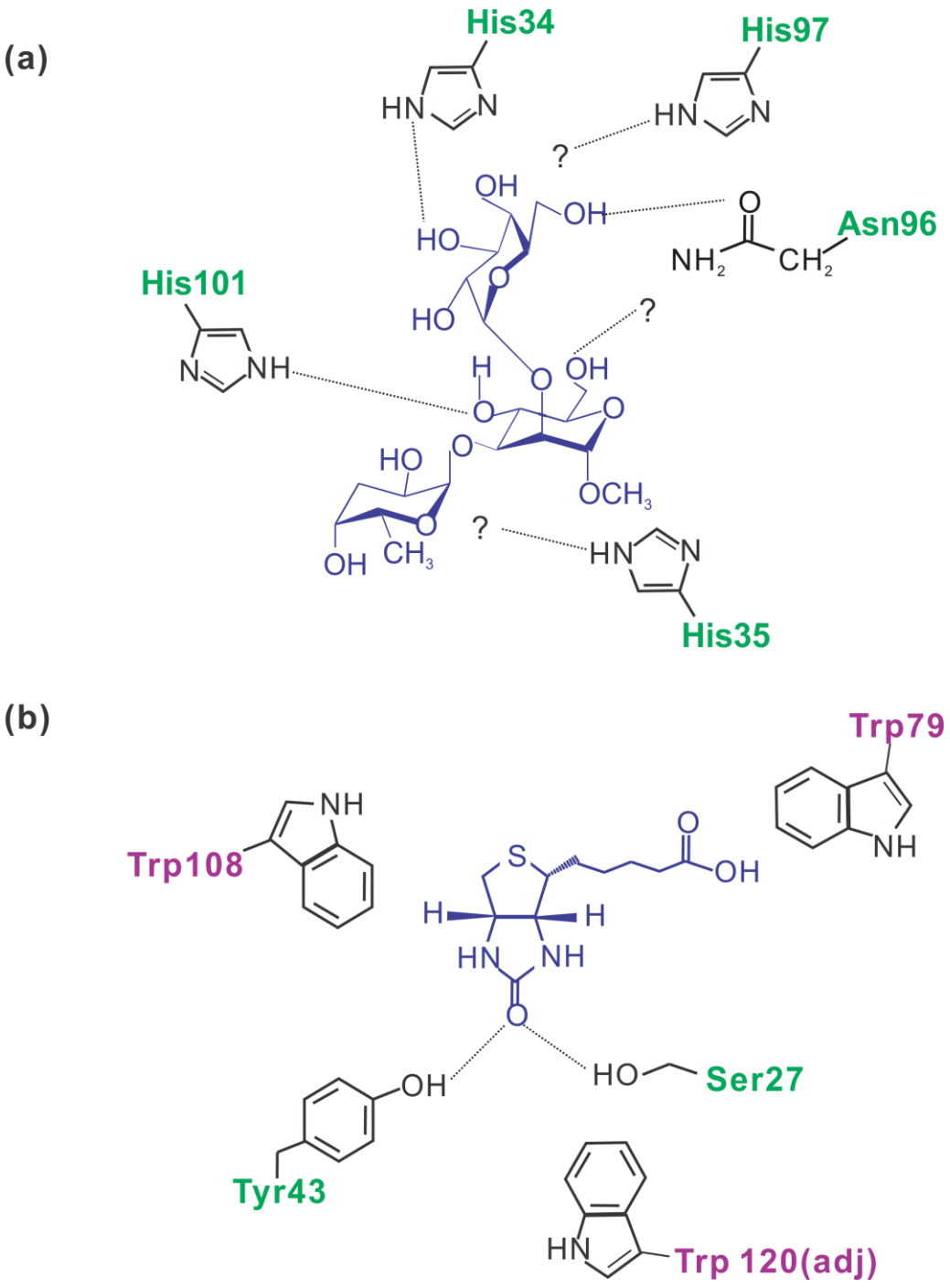
(a)
His34
His97
Asn96
His101
His35
(b)
Trp79
Trp108
Ser27
Tyr43
Trp 120(adj)

Figure 1

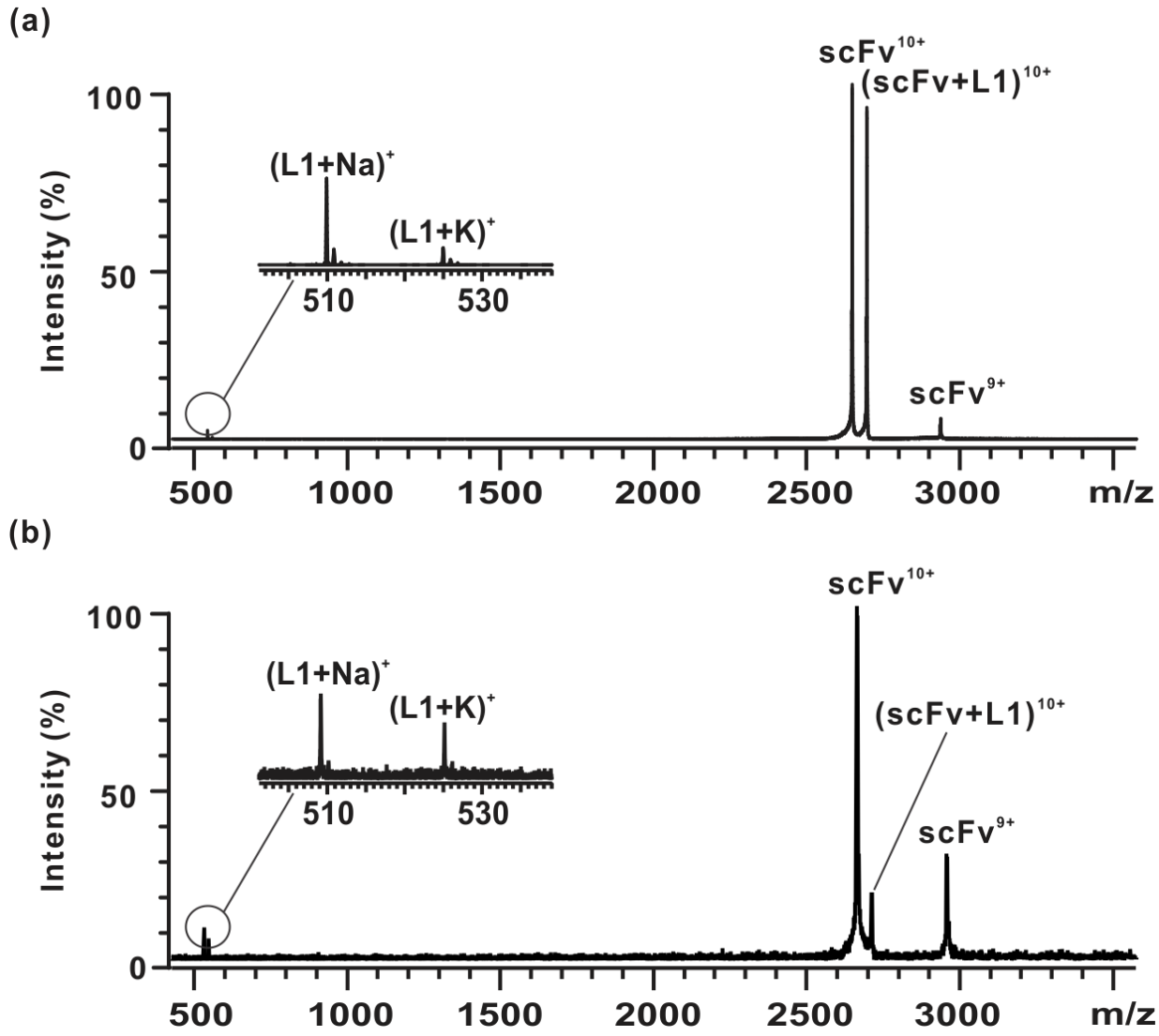
(a)
100
50
0
Intensity (%)
(L1+Na)+
(L1+K)+
510
530
scFv10+
(scFv+L1)10+
scFv9+
500
1000
1500
2000
2500
3000
m/z
(b)
100
50
0
Intensity (%)
(L1+Na)+
(L1+K)+
510
530
scFv10+
(scFv+L1)10+
scFv9+
500
1000
1500
2000
2500
3000
m/z

Figure2

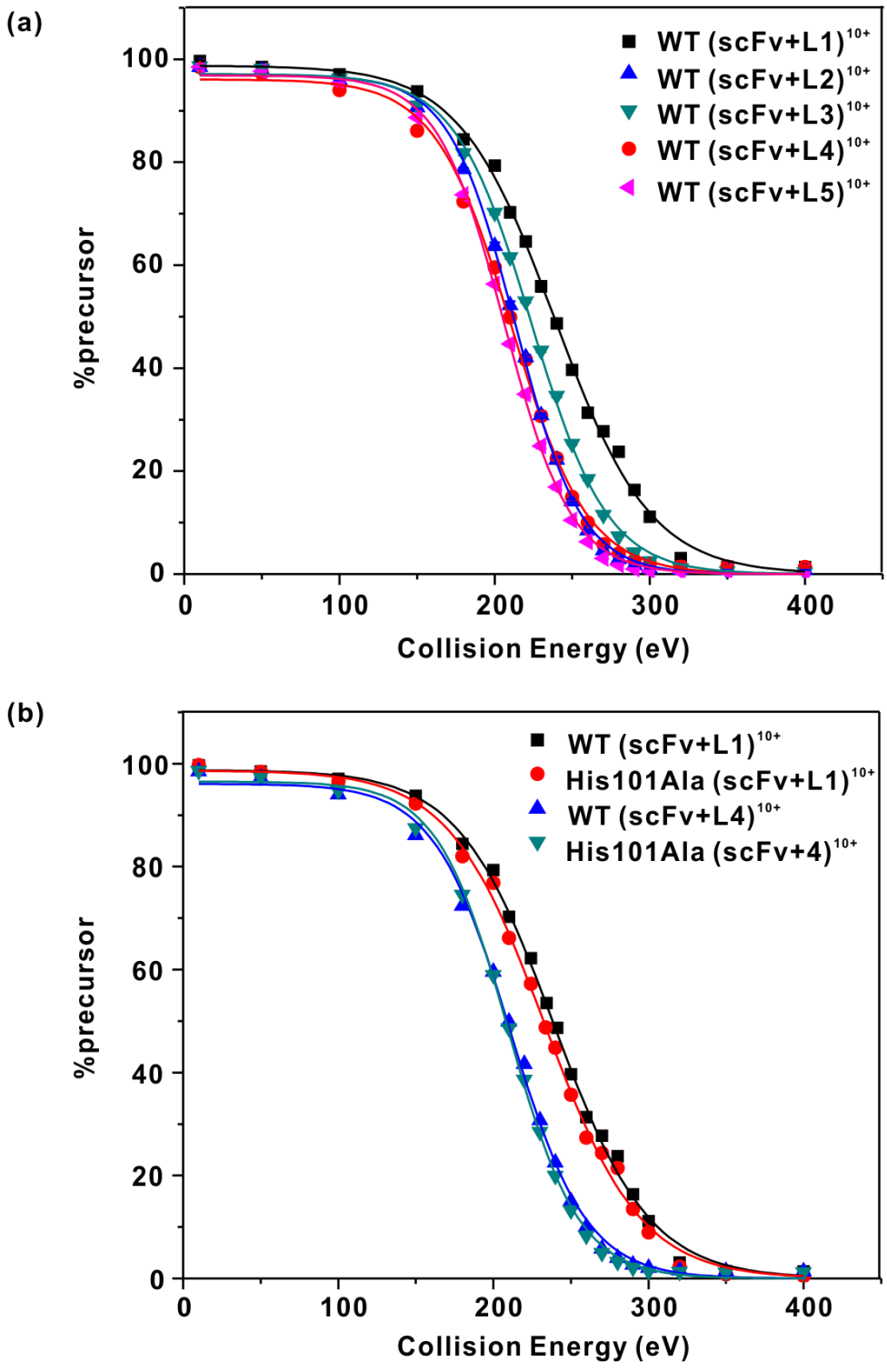
(a)
WT (scFv+L1)10+
WT (scFv+L2)10+
WT (scFv+L3)10+
WT (scFv+L4)10+
WT (scFv+L5)10+
%precursor
Collision Energy (eV)
(b)
WT (scFv+L1)10+
His101Ala (scFv+L1)10+
WT (scFv+L4)10+
His101Ala (scFv+4)10+
%precursor
Collision Energy (eV)

Figure 3

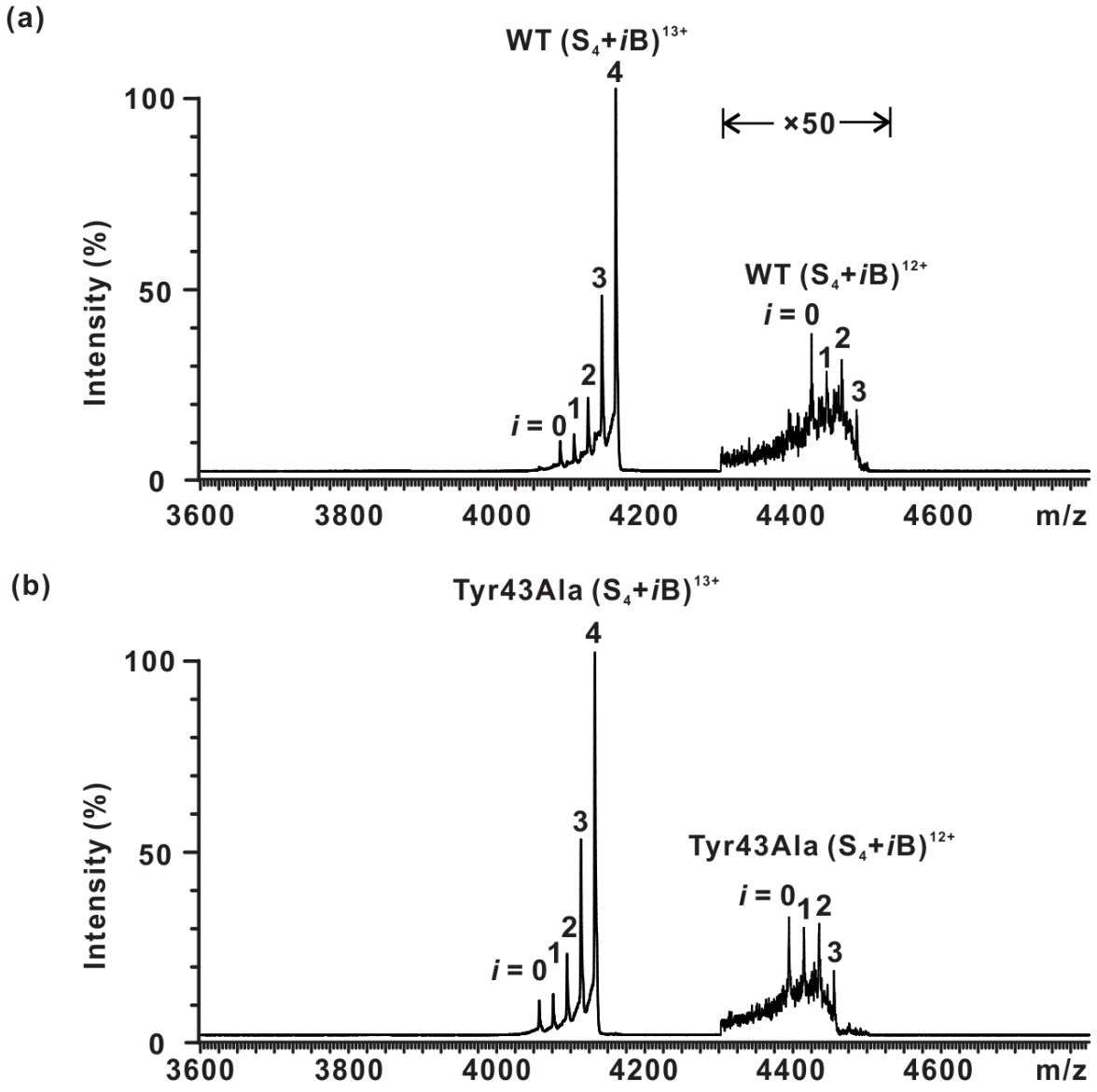
(a)
WT (S4+iB)13+
4
100
×50
Intensity (%)
50
3
WT (S4+iB)12+
i = 0
2
1
2
1
3
i = 0
0
3600
3800
4000
4200
4400
4600
m/z
(b)
Tyr43Ala (S4+iB)13+
4
100
3
50
Tyr43Ala (S4+iB)12+
i = 0
1 2
2
1
3
i = 0
0
3600
3800
4000
4200
4400
4600
m/z

Figure 4

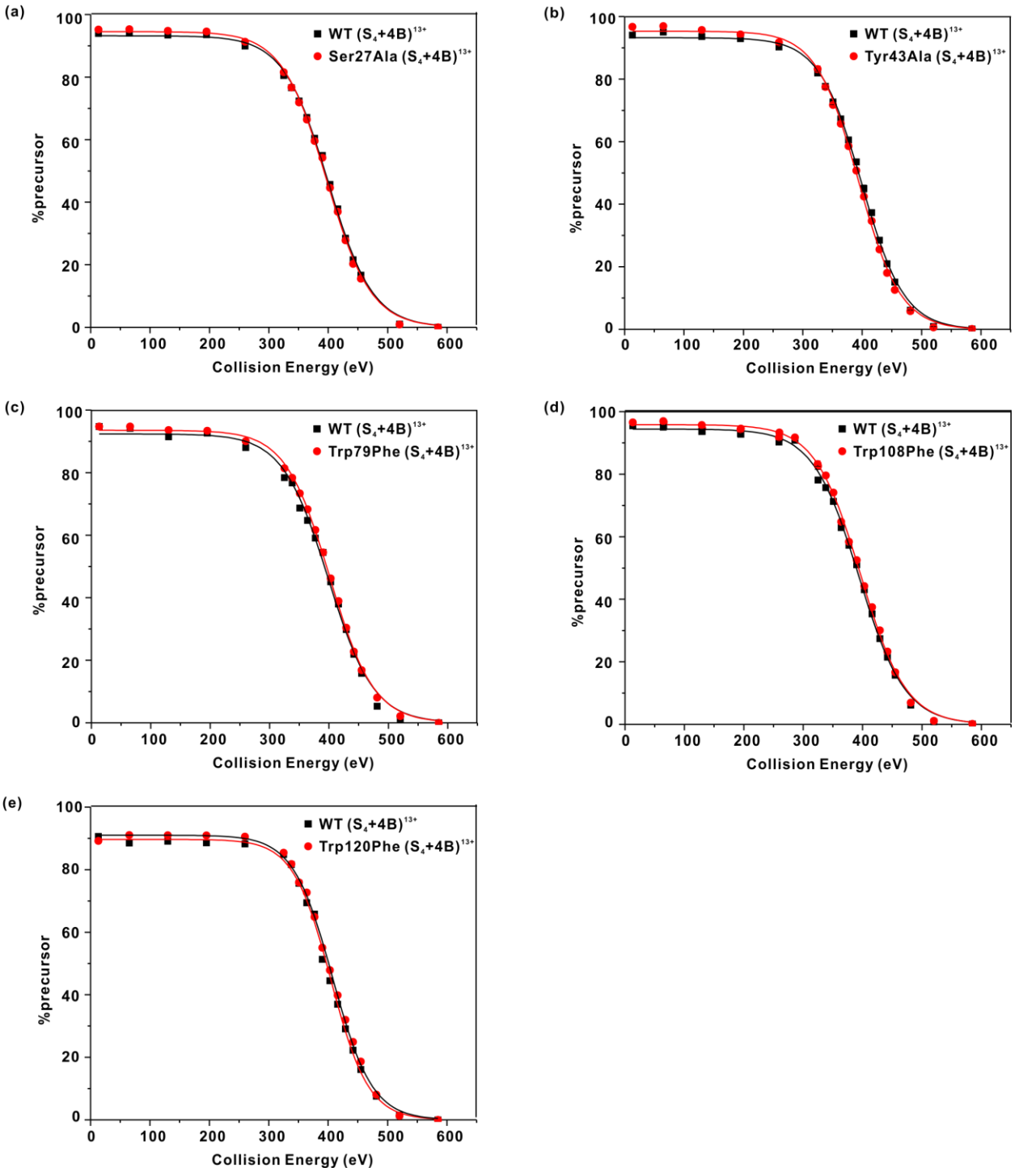
(a)
WT $(S_4+4B)^{13+}$
Ser27Ala $(S_4+4B)^{13+}$
%precursor
Collision Energy (eV)
(b)
WT $(S_4+4B)^{13+}$
Tyr43Ala $(S_4+4B)^{13+}$
%precursor
Collision Energy (eV)
(c)
WT $(S_4+4B)^{13+}$
Trp79Phe $(S_4+4B)^{13+}$
%precursor
Collision Energy (eV)
(d)
WT $(S_4+4B)^{13+}$
Trp108Phe $(S_4+4B)^{13+}$
%precursor
Collision Energy (eV)
(e)
WT $(S_4+4B)^{13+}$
Trp120Phe $(S_4+4B)^{13+}$
%precursor
Collision Energy (eV)

Figure 5

Supplementary Material for:

Mapping Protein-Ligand Interactions in the Gas Phase using a Functional Group Replacement Strategy. Comparison of CID and BIRD Activation Methods

Lu Deng, Elena N. Kitova, and John S. Klassen

Table S1. Comparison of experimentally determined collision cross sections (Ω) for the gaseous $(scFv + L1)^{n+}$ ions, where n = 9 – 11, with the Ω value calculated for crystal structure reported for the (scFv + L1) complex (protein ID: 1MFA) [S1].

Charge state (n)	$(scFv + L1)^{n+}$ Ω (nm^2)
11	22.68 ± 0.01 [a]
10	22.46 ± 0.04 [a]
9	21.86 ± 0.05 [a]
Average	22.33 ± 0.43 [b]
Crystal structure	23.24 ± 0.36 [c]

a. Uncertainty corresponds to the standard deviation of three replicate measurements. b. Uncertainty corresponds to the standard deviation of the Ω values determined at charge states +9, +10 and +11. c. Ω was determined from crystal structure (protein ID: 1MFA) [S1] using Mobcal [S2] and the trajectory method; the reported error corresponds to one standard deviation of values from replicate (10) calculations.

Table S2. Comparison of Ec_{50} values determined for the dissociation of protonated $(scFv + L)^{10+}$ ions at different trap pressure (P_{trap} = 4 (1.5×10^{-2} mbar) and 8 (2.8×10^{-2} mbar)).

L	P_{trap}	Ec_{50} [a] (eV)	ΔEc_{50} [b] (eV)
L1	4	213.1 ± 1.0	-
L2	4	195.4 ± 0.6	17.7 ± 1.5
L3	4	210.5 ± 0.6	2.6 ± 1.2
L4	4	182.1 ± 0.9	31.0 ± 1.3
L5	4	182.2 ± 0.8	30.9 ± 1.3
L1	8	235.2 ± 1.0	-
L2	8	224.1 ± 1.7	11.1 ± 1.9
L3	8	225.5 ± 0.6	9.7 ± 1.2
L4	8	197.2 ± 0.8	38.0 ± 1.3
L5	8	197.2 ± 0.7	38.0 ± 1.2

a. Errors correspond to the uncertainties of Ec_{50} values (δEc_{50}), which were calculated using error propagation. b. $\Delta Ec_{50} = Ec_{50}(scFv+L1) - Ec_{50}(scFv+L)$.

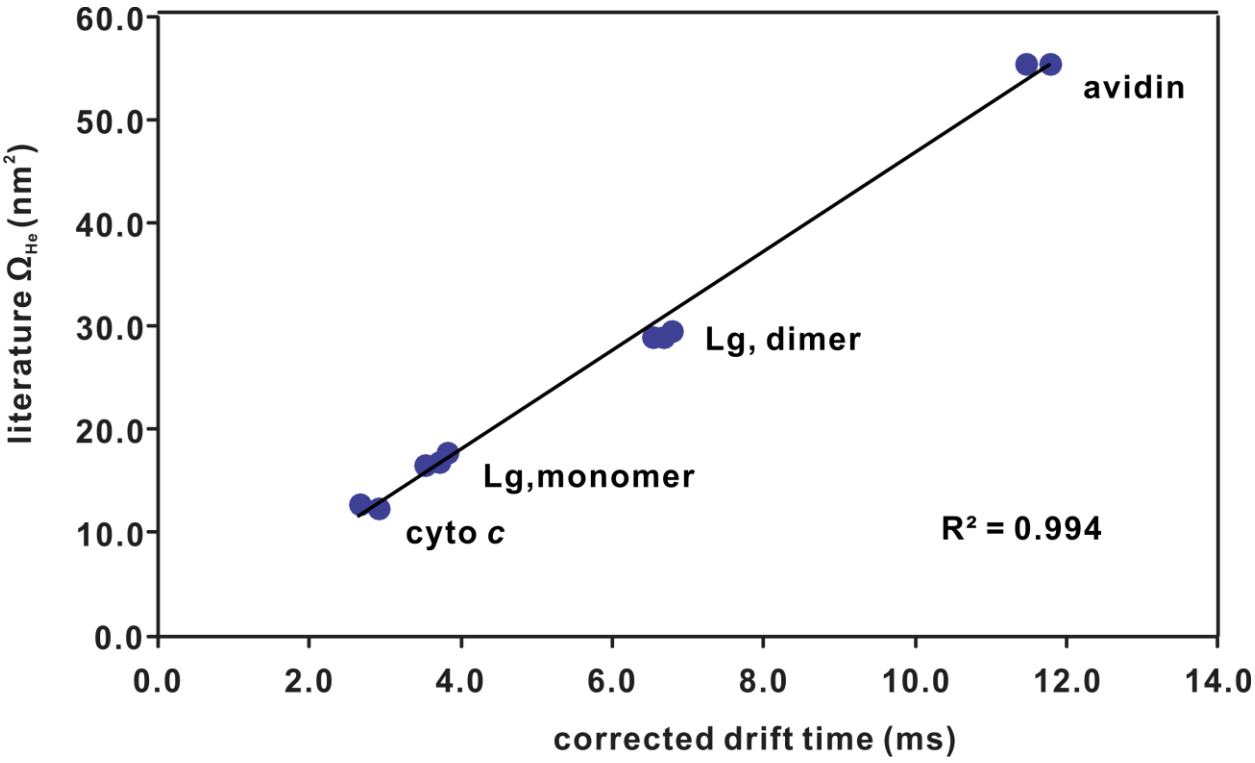

Figure S1. Calibration curve, based on the calibrants cyto *c*, Lg, and Avidin, displayed as a linear plot of literature Ω_{He} values and corrected drift times.

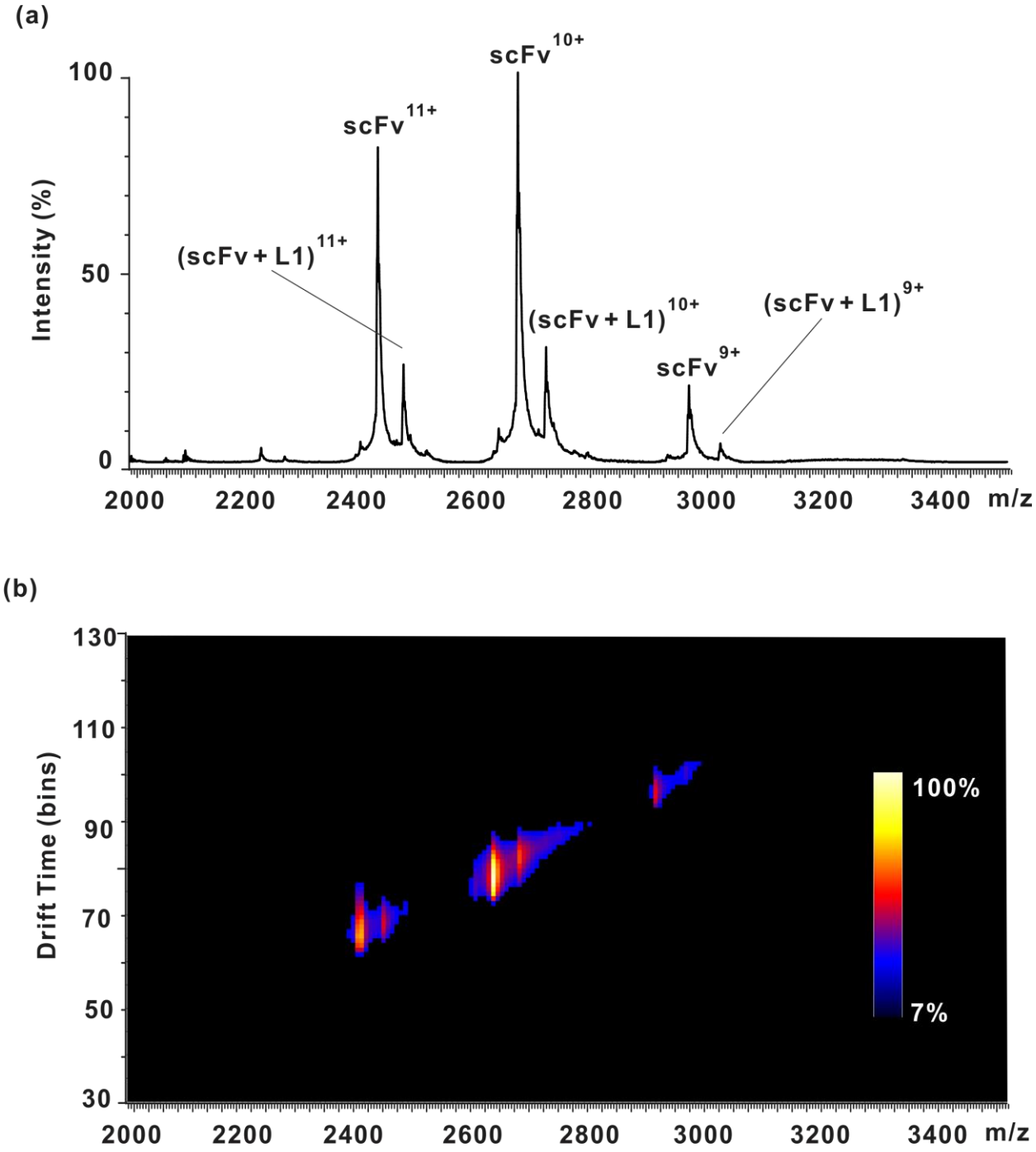

Figure S2. (a) ESI mass spectrum acquired for a solution of scFv (8 µM), L1 (5 µM) and 10 mM ammonium acetate (pH 6.8). (b) Ion mobility heat map of arrival time distribution versus *m/z.* The normalized ion intensities (from 7% to 100%) are represented using the indicated colour scale.

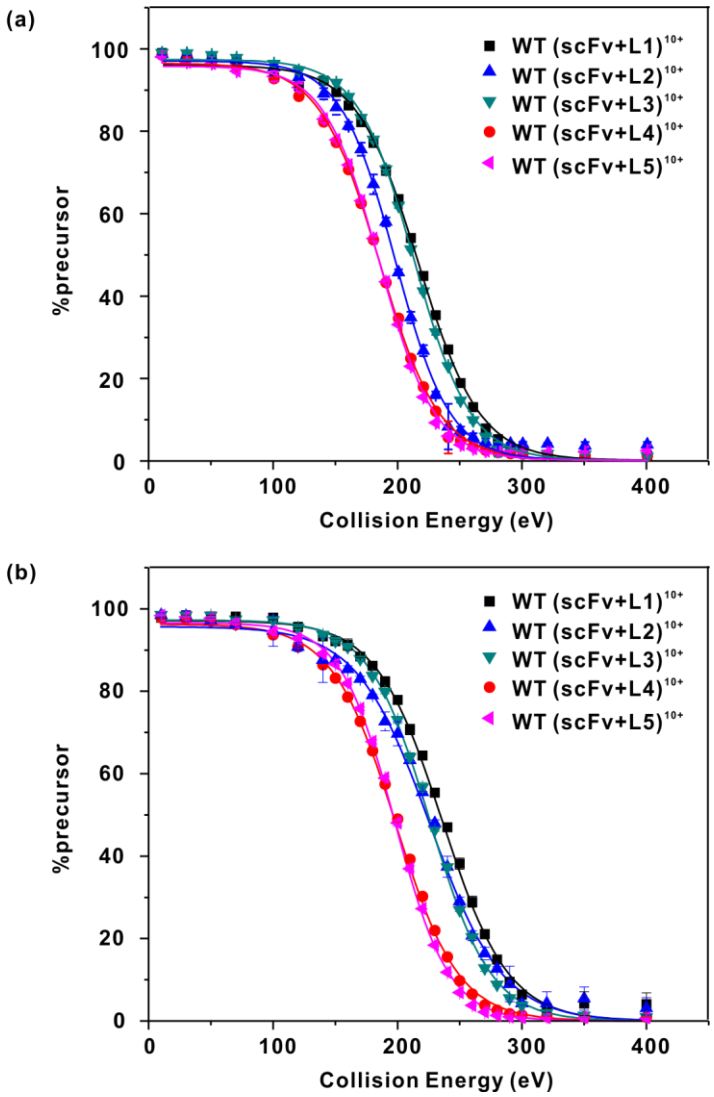

Figure S3. (a) CID profiles measured for the protonated WT (scFv + L)$^{10+}$ ions, where L= L1 – L5, at P_{trap} = 4. (b) CID profiles measured for the protonated WT (scFv + L)$^{10+}$ ions, where L= L1 – L5, at P_{trap} = 8. The solid curves were determined from sigmoid fitting to the collision energy-dependent %precursor values.

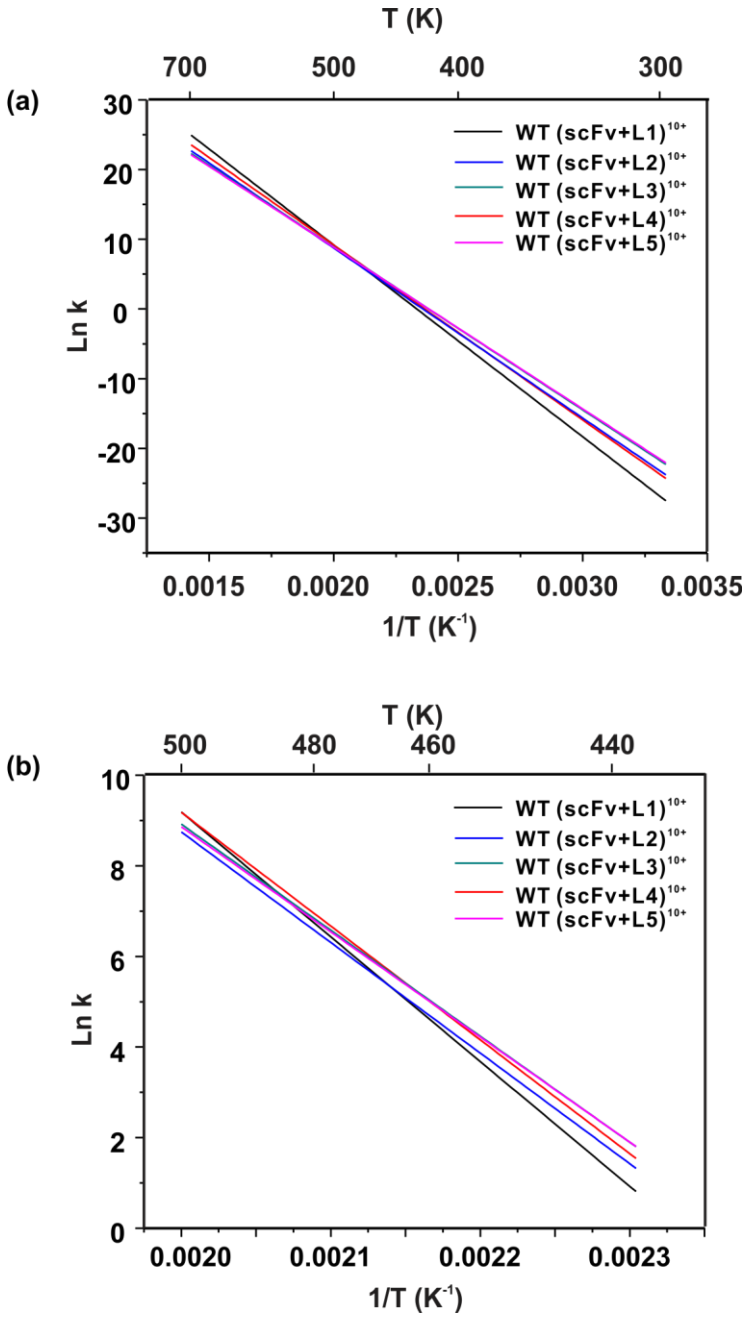

Figure S4. Arrhenius plots for the dissociation of WT (scFv + L)$^{10+}$ ions, where L= L1 – L5, calculated from the E_a and A values reported in [S3] in the temperature range (a) 300 K to 700K and (b) 440 K to 500 K.

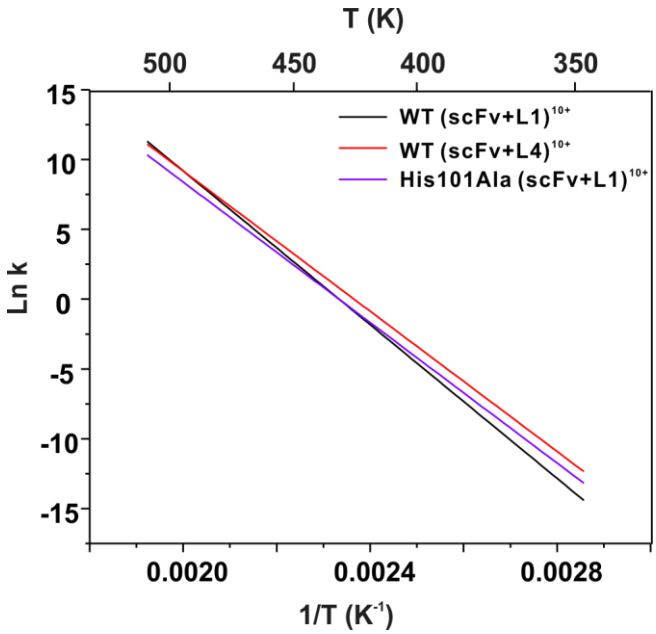

Figure S5. Arrhenius plots for the dissociation of WT $(scFv + L1)^{10+}$ ions, WT $(scFv + L4)^{10+}$ ions and His101Ala $(scFv + L1)^{10+}$ ions, calculated from the E_a and A values reported in [S3] in the temperature range 350 K to 520K.

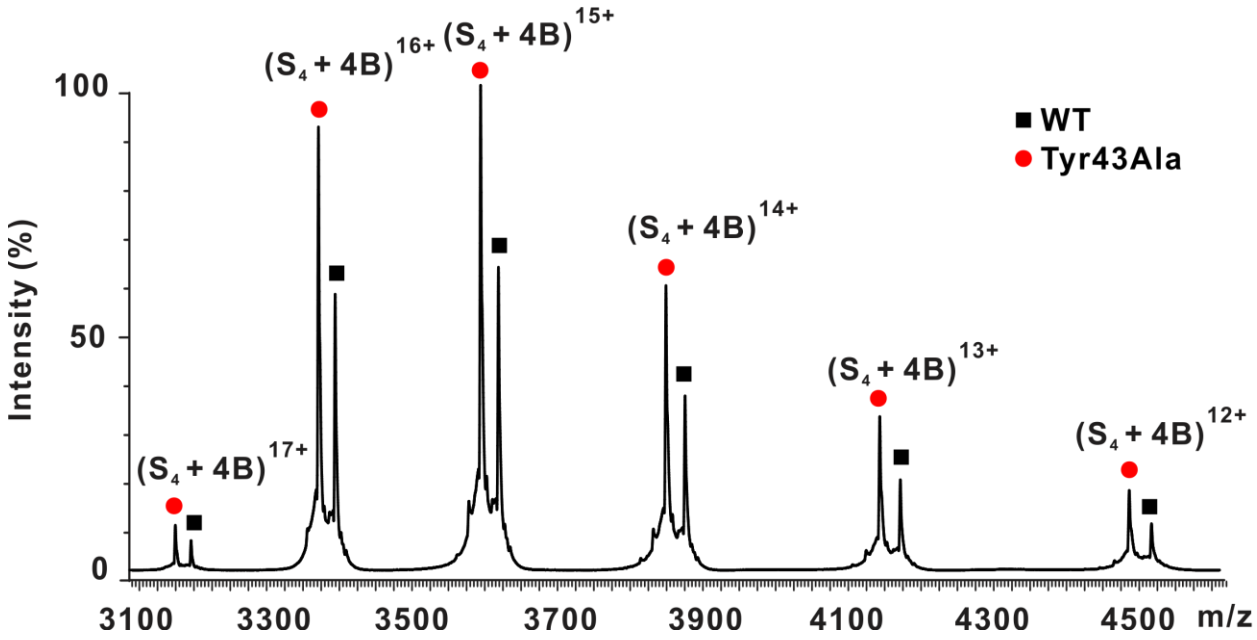

Figure S6. ESI mass spectrum acquired for a neutral aqueous ammonium acetate (10 mM) solution of WT S_4 (8 μM), Tyr43Ala S_4 (10 μM), B (80 μM) and imidazole (5 mM).

Reference

S1. Zdanov, A., Li, Y., Bundle, D.R., Deng, S.J., MacKenzie, C.R., Narang, S.A., Young, N.M., Cygler, M.: Structure of a single-chain antibody variable domain (Fv) fragment complexed with a carbohydrate antigen at 1.7-A resolution. *Proc. Natl. Acad. Sci. U. S. A.* **91,** 6423-6427 (1994)

S2. Mesleh, M.F., Hunter, J.M., Shvartsburg, A.A., Schatz, G.C., Jarrold, M.F.: Structural Information from Ion Mobility Measurements: Effects of the Long-Range Potential. *The Journal of Physical Chemistry* **100,** 16082-16086 (1996)

S3. Kitova, E.N., Seo, M., Roy, P.-N., Klassen, J.S.: Elucidating the Intermolecular Interactions within a Desolvated Protein−Ligand Complex. An Experimental and Computational Study. *J. Am. Chem. Soc.* **130,** 1214-1226 (2008)